Journal of Integrative Neuroscience

J. Integr. Neurosci. **2025**; 24(6): 39116
https://doi.org/10.31083/JIN39116

Original Research

Muscone Protects Against Ferroptosis-Induced Injury in Models of Acute Ischemic Stroke by Modulating Snap25 Protein

Ruijia You[1,†], Bin Sun[1,†], Jing Luo[1], Guanhua Hu[1], Nan Shao[1], Wenwen Si[1,*]

[1]School of Integrated Chinese and Western Medicine, Anhui University of Chinese Medicine, 230012 Hefei, Anhui, China
*Correspondence: siwenwen2008@163.com (Wenwen Si)
[†]These authors contributed equally.
Academic Editor: Zhong Chen
Submitted: 18 March 2025 Revised: 26 April 2025 Accepted: 30 April 2025 Published: 19 June 2025

Abstract

Background: Acute ischemic stroke (AIS) is one of the leading critical neurological conditions globally, resulting in significant adult mortality and disability. Previous studies have demonstrated a close relationship between AIS and the ferroptosis signaling pathway. Muscone, the primary active small-molecule component of musk, is a traditional Chinese medicine that exhibits significant pharmacological effects in reducing stroke injury. However, there is still only limited research on whether muscone can modulate ferroptosis-related injury in AIS, and on the underlying regulatory molecular mechanisms. **Methods**: We utilized a transmission electron microscope and concurrently performed assays for glutathione peroxidase 4 (GPX4) activity, glutathione (GSH), reactive oxygen species (ROS), lipid peroxides, as well as cell viability and live/dead cell staining to investigate alterations in ferroptosis levels. RNA sequencing, bioinformatics analysis, and western blot (WB) assays were employed to evaluate the changes in synaptosome-associated protein 25 kDa (Snap25) expression levels. Furthermore, molecular docking, surface plasmon resonance (SPR) detection, and molecular dynamics (MD) simulation were implemented to examine the binding affinity and interaction between muscone and Snap25. **Results**: RNA sequencing technology, bioinformatics analysis, and WB assays revealed that Snap25 was specifically downregulated under simulated AIS conditions. Snap25 knockdown and overexpression experiments were also conducted to elucidate the molecular mechanism by which muscone modulates Snap25 expression, thereby mitigating ferroptosis injury in AIS. Additionally, the results of molecular docking, SPR detection, and MD simulations indicate that muscone has multiple binding sites that allow it to bind directly to the Snap25 protein, thereby stabilizing the protein structure. **Conclusions**: Our findings suggest that muscone produces an anti-AIS effect in the context of AIS injury by increasing Snap25 protein expression, thus reducing ferroptosis. This investigation offers insight into the anti-stroke mechanism of muscone and introduces a promising new treatment option for clinical AIS management.

Keywords: muscone; ischemic stroke; ferroptosis; Snap25; MCAO/R

1. Introduction

Stroke is still one of the primary causes of death and disability in the adult population globally [1–3]. The majority of cases are due to acute ischemic stroke (AIS), distinguished by sudden onset, fast progression, and complex clinical manifestations [4,5]. AIS results in disrupted blood supply, inadequate nutrition, and the accumulation of toxic substances which leads to severely impaired nerve function [6–8]. The most frequently used treatment for AIS is revascularization therapy. However, since the time window for revascularization treatment is narrow, a substantial proportion of AIS patients do not derive any benefit [9,10]. Therefore, developing safer and more effective drugs for treating AIS has major clinical significance.

Ischemic stroke represents a complex and highly heterogeneous condition. The primary subtypes of ischemic stroke include atherosclerotic thrombotic infarction, cardiogenic embolic stroke, and lacunar infarction, each of which is characterized by distinct etiologies and risk factors [11]. Atherosclerotic thrombotic infarction is predominantly associated with large artery atherosclerosis, and shows a higher prevalence in adult males. Patients with this subtype typically experience prolonged hospital stays and face an elevated short-term risk of recurrence. Cardioembolic stroke is primarily attributable to cardiac pathologies, and occurs more frequently in elderly women. Individuals affected by this subtype often present with severe symptoms at onset, encounter numerous complications, and have a poor prognosis [12]. Lacunar infarction is commonly related to small vessel disease and is prevalent among hypertensive patients. This subtype generally manifests with milder symptoms and has a more favorable prognosis [13].

AIS involves various mechanisms of disease progression, including excitotoxicity, oxidative stress, inflammatory response, and ferroptosis [14–16]. Current research has shown that functional and structural damage to AIS neurons is closely associated with the level of oxidative stress. Specifically, the elevated concentration of reactive oxygen species (ROS) has been identified as the primary factor contributing to the substantial increase in oxidative stress [17,18]. ROS-mediated lipid peroxide (LPO) damage is a primary mechanism of cellular injury, resulting in altered

physiological properties of the cell membrane and increased membrane permeability during AIS, ultimately leading to neuronal cell death [19,20]. Abnormally elevated levels of ROS and lipid peroxidation are critical indicators of the ferroptosis pathway [21,22]. Ferroptosis is a type of cell death that relies on iron and is initiated by excessive damage from lipid peroxidation, resulting in elevated oxidative stress and eventual cell death [23–25]. Recent investigations have underscored the pivotal function of ferroptosis in the pathogenesis of neurological disorders [26,27]. Nevertheless, the regulatory mechanisms underlying ferroptosis in AIS-induced injury remain incompletely understood.

Musk is a traditional Chinese medicine (TCM) utilized extensively in treating cerebrovascular disorders such as ischemic stroke. Muscone is a crucial constituent of musk and the primary physiologically active substance. It has been demonstrated to decrease cerebral infarct volume and neurological dysfunction [28,29]. Synaptosome-associated protein 25 (Snap25) is a widely expressed neurotransmitter transport protein in neuronal cells that is pivotal in neurotransmission, primarily facilitating synaptic vesicle fusion and neurotransmitter release [30]. Snap25 has been linked to the development of multiple neurological conditions, such as attention deficit hyperactivity disorder [31], Alzheimer's disease [32], and developmental and epileptic encephalopathy [33]. Recent study has demonstrated that Snap25 can mitigate postoperative cognitive dysfunction by promoting mitochondrial autophagy and reducing pyroptosis-induced damage in hippocampal neurons [34]. In the present study, RNA sequencing and western blot (WB) experiments revealed that muscone significantly upregulates Snap25 expression under AIS conditions. This prompted us to investigate whether muscone reduces ferroptosis levels in AIS by modulating Snap25, an area that to our knowledge has yet to be explored.

Our study utilized 2,3,5-Triphenyl-Tetrazolium Chloride (TTC) and live/dead cell staining to assess the damage level in a rat model of middle cerebral artery occlusion/reperfusion (MCAO/R), and in oxygen-glucose deprivation/reperfusion (OGD/R) injury of PC12 cells. The ferroptosis level was determined by evaluating the activity of glutathione peroxidase 4 (GPX4) and the concentrations of glutathione (GSH), ROS and LPO, as well as by observing changes in mitochondrial morphology. We employed a combination of experimental approaches, including molecular docking, surface plasmon resonance (SPR) detection, molecular dynamics (MD) simulation, RNA interference (RNAi), and protein overexpression to explore the mechanism by which muscone regulates ferroptosis in AIS. The findings of this study should increase our comprehension of the underlying mechanisms of AIS injury and the therapeutic effects of muscone, thus offering promising therapeutic approaches for AIS clinical management.

2. Materials and Methods

2.1 Serum Biochemical Indexes

Animal trials received approval from the Animal Ethics Committee, Anhui University of Chinese Medicine (Hefei, China; ethical clearance number AHUCM-rats-2023126) and were conducted as per the ARRIVE instructions. Twenty-four male Sprague-Dawley rats (specific pathogen-free, SPF, Anhui Qingyuan Biotechnology Co., Ltd, Hefei, China) with a weight of 230–260 g and aged 8–9 weeks were equally assigned to four groups in a random manner: sham control, M3 (muscone 3 mg/kg), M9 (muscone 9 mg/kg), and M18 (muscone 18 mg/kg). Pharmaceutical-grade muscone (S25595, Yuanye Biotechnology, Shanghai, China) was delivered intravenously via the tail vein. Following a 24-h post-administration period, anesthetization of rats was conducted with 5% isoflurane (R510-22-10, RWD Life Science Co., Ltd, Shenzhen, China) and 2.5% isoflurane was used to maintain them. Terminal blood collection (5 mL) was performed via abdominal aortic puncture prior to euthanasia by cervical dislocation under sustained anesthesia. The blood specimens were spun at 1800 g for 15 min to isolate serum components. Hepatic and renal biomarkers (ALT, alanine aminotransferase; AST, aspartate aminotransferase; BUN, blood urea nitrogen; Cr, creatinine) were quantified using a HITACHI 7600-020 Automatic Analyzer (Hitachi High-Technologies Corporation, Tokyo, Japan) and following standardized protocols.

2.2 Preparing the Rat MCAO/R Model

Sprague-Dawley rats (n = 60) with the age of 8–9 weeks (230–260 g body weight) were classified into five experimental cohorts in a random manner: sham-operated controls, MCAO/R model group, MCAO/R with low-dose muscone (3 mg/kg), MCAO/R with high-dose muscone (9 mg/kg), and MCAO/R with edaravone (3 mg/kg) treatment. The MCAO/R model was prepared as illustrated in previous work [35,36]. A median cervical incision was made to expose the left common (CCA), internal (ICA), and external carotid arteries (ECA). The CCA was clamped, the distal ECA ligated, and a micro-incision made at the proximal ECA. A silicone-coated thread embolus (907-00029-01, RWD Life Science Co., Ltd) was inserted via the ECA, advanced into the ICA through the CCA bifurcation, and stopped upon resistance. After securing the embolus, ischemia was sustained for 1 h, followed by thread withdrawal. The proximal ECA was ligated, the CCA clamp removed, and reperfusion initiated. A laser Doppler flowmeter (PF5010, Perimed Co., Ltd, Stockholm, Sweden) was utilized for monitoring the regional cerebral blood flow (rCBF). A >75% rCBF lessening throughout ischemia indicated effective middle cerebral artery occlusion, and recovery to >75% of baseline confirmed reperfusion. Blood flow restoration was achieved through careful suture removal, with subsequent tail vein administration of mus-

cone. The preparation and administration steps of the MCAO/R model have been completed. The animal's body temperature throughout the experiment and until awaking from anesthesia was about 36.5 °C.

2.3 Neurological Deficit Scores

The Longa score scale was utilized to evaluate the neurological deficit in MCAO/R rats as described previously [36]. The neurological deficit evaluation was performed at the 24th hour after blood perfusion was restored in MCAO/R rats.

2.4 2,3,5-Triphenyl-Tetrazolium Chloride (TTC) Staining

Following the establishment of the AIS model, MCAO/R rats were euthanized by rapid decapitation, and their whole brains extracted, and then cutting them was conducted into slices of 2 mm thickness on ice. Staining the slices was then conducted (37 ℃, 20 min) with 2% TTC dye solution (BB-44549, Bestbio Co., Ltd, Shanghai, China) and photographed. Infarct areas were identified as pale regions in the cerebral hemisphere, and the percentage of infarct size was calculated using Image J software (v1.52a; NIH, Bethesda, MD, USA).

2.5 RNA-Seq and Bioinformatics Analysis

Total RNA extraction was conducted from both healthy and infarcted cortical tissues via Trizol reagent (15596026CN, Invitrogen, Carlsbad, CA, USA). Following library preparation and alignment, genes were classified as differentially expressed genes (DEGs) if they exhibited a $|\log2(\text{Fold-Change})| > 1$ and a p-value < 0.05. Gene Ontology (GO) analysis was carried out on DEGs to detect their biological process (BP), cellular component (CC), and molecular function (MF), with heatmaps illustrating expression differences between groups.

2.6 Hematoxylin-eosin (HE) Staining

After adequate fixation, the tissues/cells were stained with HE staining kits (C0105S, Beyotime Biotechnology, Shanghai, China). The degree of damage in the cortex of rats was then assessed via an inverted microscope (IX81, Olympus, Tokyo, Japan).

2.7 WB Analysis

In ice-cold RIPA buffer (89900, Thermo Fisher Scientific, Waltham, MA, USA), cortical tissue and PC12 cells were lysed. Beyotime Biotechnology's BCA kit (P0012, Shanghai, China) was used to measure total protein. After being separated using sodium dodecyl sulfate polyacrylamide gel electrophoresis (SDS-PAGE), protein samples weighing 30 µg were transferred to polyvinylidene fluoride (PVDF) membranes with a thickness of 0.45 µm. Before incubating with primary and secondary antibodies, a 1-h blockage of membranes was conducted with 5% bovine serum albumin at room temperature. Located in Wuhan, China, ProteinTech is the source of the anti-Snap25 antibody (1:5000, 14903-1-AP). Abcam (Cambridge, UK) provided the following antibodies: GAPDH (1:5000, ab181602), horseradish peroxidase (HRP, 1:5000, ab6721), and ab6789, which are goat anti-rabbit and mouse IgG H&L. The enhanced chemiluminescence (ECL) substrate (34580, Pierce, Thermo Fisher Scientific) was used for band visualization. The gray value of the protein band was calculated by using the Image J software (v1.52a; NIH, Bethesda, MD, USA). The original western blots can be found in the **Supplementary Material**.

2.8 Cell Viability Assessment

The PC12 cell viability was strictly assessed with the CCK-8 assay kit (C0037, Beyotime Biotechnology) as per the manufacturer's guidelines. Subsequently, cell viability was evaluated via an enzymatic reader at 450 nm. The formula used to determine cell viability was: % cell viability = OD (treatment)/OD (control) $\times$ 100%.

2.9 OGD/R Injury

PC12 cells were brought from the American Type Culture Collection (Catalogue no. CRL-1721.1TM, ATCC, Manassas, VA, USA) and cultivated in RPMI 1640 medium (Catalogue no. 11875093, Invitrogen) with 5% fetal bovine serum (Catalogue no. A5670701, Invitrogen). The cells underwent regular authentication through morphological examination and short tandem repeat (STR) authentication and were checked for Mycoplasma contamination. The mycoplasma contamination detection kit (Beyotime Biotechnology, Cat. No. C0297S) was used to test cell lines for mycoplasma, and they were found to be negative. PC12 cells were cultivated into 6-well plates (2×10^5 cells/well) and then incubation was conducted at 37 °C with 5% CO_2. Before oxygen-glucose deprivation, PBS was employed to rinse the cells that were then cultivated in glucose-free RPMI 1640 medium and incubated in an anaerobic chamber at 37 °C with 5% CO_2 and 95% N_2 for 6 h. Subsequently, replacing the medium was conducted with regular medium containing different drug concentrations, and the incubation of cells was conducted under normal circumstances at 37 °C for 24 h to simulate reperfusion.

2.10 ROS Measurement

ROS concentrations in cortical tissue were assessed via a ROS detection kit (BB-470515, BestBio Co., Ltd.) as per the guidelines of the manufacturer. Fluorescence was detected at 510 nm (excitation) and 610 nm (emission) via a SpectraMax iD3 microplate reader (Molecular Devices, Sunnyvale, CA, USA). Intracellular ROS in PC12 cells was evaluated with the Cell ROS Assay Kit (S0033S, Beyotime Biotechnology). Cells (3×10^4/well) were seeded in 96-well plates, and fluorescence was assessed at 485 nm (excitation) and 520 nm (emission).

2.11 Lipid Peroxidation Measurement

The TBARS Assay Kit (S0131M, Beyotime Biotechnology, Shanghai, China) was utilized to measure lipid peroxidation in cortical tissue and PC12 cells. For this analysis, cortex tissue samples (25 mg) and cell suspensions (1×10^6 cells) were homogenized or lysed, respectively, using the lysis buffer provided in the kit. Following centrifugation at 4 ℃ for 10,000 g and 10 min, the supernatant was gathered for subsequent evaluation. The supernatant, thiobarbituric acid (TBA) detection reagent, and color-developing reagent were added to a 96-well plate at a ratio of 1:1:8. After mixing, heating for 15 min at 100 ℃, and cooling rapidly to room temperature with water, the absorbance was calculated at 532 nm via a microplate reader (MK3, Thermo Fisher Scientific, Waltham, MA, USA).

2.12 Transmission Electron Microscopy (TEM)

The brain cortex tissue of rats, as well as cultured PC12 cells, were stabilized at 4 ℃ for 2 h with 2.5% glutaraldehyde (Catalogue no. G5882, Sigma-Aldrich, St. Louis, MO, USA). Subsequently, the mitochondrial morphology was examined by TEM (JEM-1400 PLUS, Tokyo, Japan).

2.13 Staining of Live/Dead Cells

The LIVE/DEAD™ imaging kit from Thermo Fisher Scientific (L3224, Invitrogen) was used as recommended by the manufacturer to assess cell mortality across all experimental groups. PC12 cells were photographed at 100× magnification using an inverted phase microscope (IX81, Olympus).

2.14 Assessment of GSH Content and GPX4 Activity

GSH content and GPX4 activity were measured in homogenized rat cortex and PC12 cell supernatants using the GSH test kit (ab138881, Abcam) and GPX4 Activity Assay Kit (E-BC-K883-M, ElabScience Biotechnology Co., Ltd, Wuhan, China), respectively, as recommended by the guidelines of the manufacturer.

2.15 Evaluation of Iron Ion Concentration

An iron content detection kit (I291, Dojindo Laboratories, Kumamoto, Japan) was used to measure the concentrations of ferrous and total iron ions in rat cortical tissue and PC12 cells, as recommended by the manufacturer. Microplate readers from Thermo Fisher Scientific were employed to calculate absorbance at 593 nm, which was subsequently used to calculate the concentrations of iron ions.

2.16 Molecular Docking Analysis

Autodock Vina 1.1.2 software (Scripps Research Institute, San Diego, CA, USA) was employed to conduct molecular docking simulation analysis. The crystal structure of Snap25 protein (Protein Data Bank (PDB) ID: 1N7S) was gained from the RCSB Protein Data Bank (https://www.rcsb.org/, USA) in PDB format. The molecular structure of muscone (ID 10947) was retrieved from the PubChem database (https://pubchem.ncbi.nlm.nih.gov) and transformed into PDB format with the PyMOL Molecular Graphics System (v 2.5.0, Schrödinger, Inc., New York, NY, USA). Finally, Autodock Vina software was employed to perform the docking study.

2.17 Detection of SPR

SPR detection was employed to assess the interaction between Snap25 protein (HY-P73634, MedChemExpress, Monmouth Junctio, NJ, USA) and muscone. Immobilization of the Snap25 protein was conducted on a Series S CM5 Sensor Chip (GE Healthcare, Washington, DC, USA) via amino coupling. Muscone solutions were prepared at numerous doses (0.3125, 0.625, 1.25, 2.5, 5, and 10 µM) using 1× PBS-P+ buffer containing 5% DMSO. Interaction analysis was conducted with a Biacore 1K instrument (Cytiva, Danahe Group, Washington, D.C., USA). The dissociation (K_D), association rate (Ka), and dissociation rate constants were subsequently determined via Biacore Insight evaluation software (version 3.0.11.15423, Cytiva, Danahe Group).

2.18 MD Simulations

MD simulations were conducted via GROMACS (v 5.1.4, Uppsala University, Uppsala, Sweden). Two systems were constructed: with ligand (Snap25 protein + muscone), and without ligand (Snap25 protein only). Topological files for the molecular structures were generated via the CHARMM-GUI (http://www.charmm-gui.org) web interface. Both systems were positioned in a cubic simulation box with applying periodic boundary circumstances, using the gmx solvate tool in GROMACS (https://www.gromacs.org, GROMACS 2023.3, KTH Royal Institute of Technology, Stockholm, Sweden). Upon completion of the simulation, various metrics were computed and analyzed.

2.19 RNAi of Snap25 in PC12 Cells

Synthetic siRNA was used to perform RNAi targeting *Snap25*. Three *Snap25*-specific siRNAs (*Snap25*-siRNA-1, *Snap25*-siRNA-2, *Snap25*-siRNA-3) and a negative control (NC) siRNA were synthesized by Hanbio Corporation (JY20220810WY-SI02, Shanghai, China). The siRNAs and NC sequences were as follows: *Snap25*-siRNA-1, UUGCUCAUCCAACAUAACCTT; *Snap25*-siRNA-2, UUAUUGAUUUGGUCCAUCCTT; *Snap25*-siRNA-3, UUCUGCUUCUUUCAUAUCCTT; NC, ACGUGACACGUUCGGAGAATT. Transfection was carried out via Lipofectamine™ 3000 (L3000015, Invitrogen, Carlsbad) with *Snap25*-siRNA-1, *Snap25*-siRNA-2, *Snap25*-siRNA-3, or NC siRNA (100 nM for each). PC12 cells were transfected for 24-h prior to further experiments.

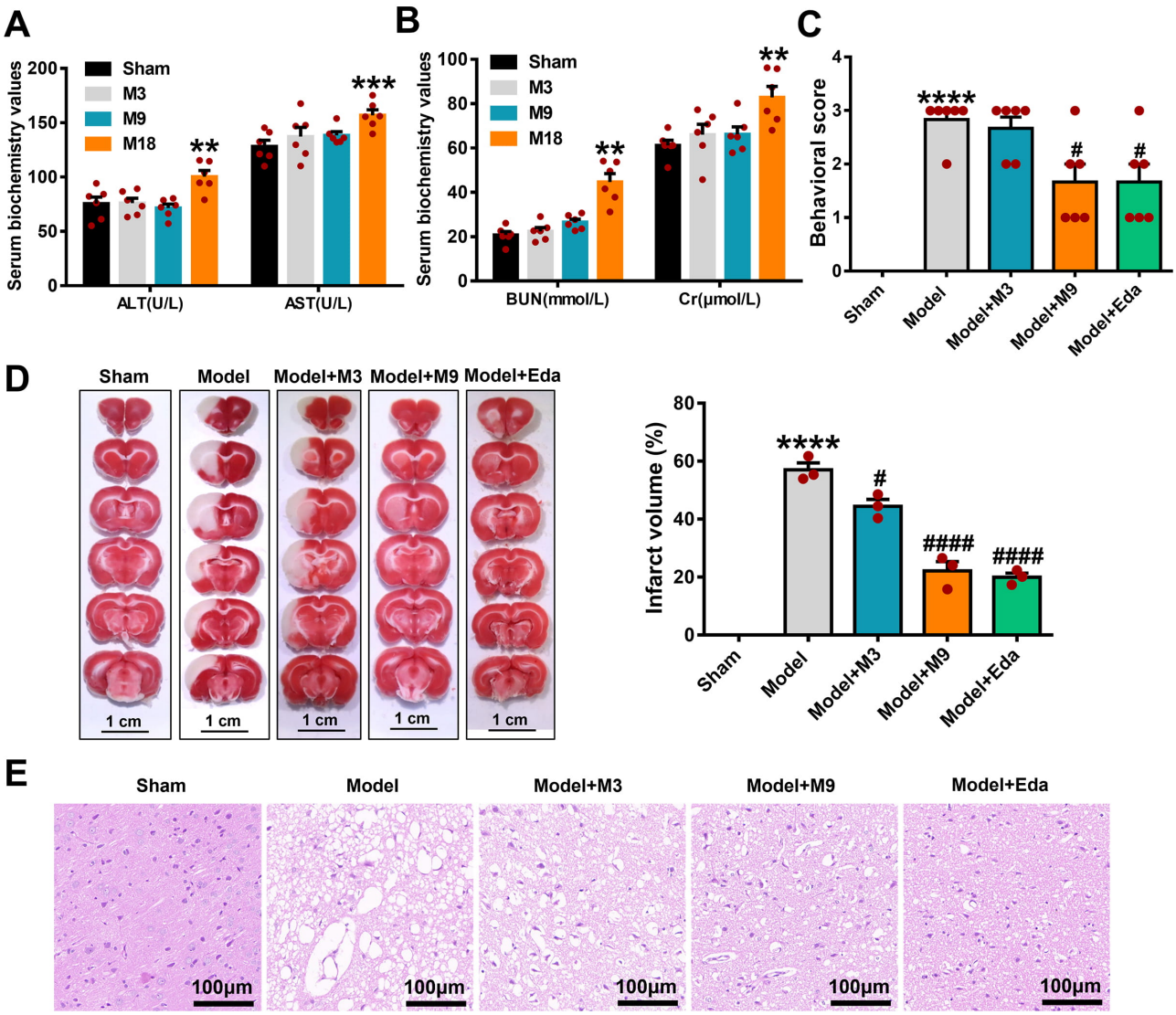

Fig. 1. Muscone mitigates acute cerebral ischemic injury in middle cerebral artery occlusion/reperfusion (MCAO/R) rats. (A) The impact of different concentrations of muscone (M3 group, 3 mg/kg; M9 group, 9 mg/kg; M18 group, 18 mg/kg) on liver function in rats, as detected by the serum biochemical index. (B) The impact of different concentrations of muscone on kidney function in rats, as detected by the serum biochemical index. (C) Muscone enhanced the neurological deficit scores in MCAO/R rats. The protective influence of muscone on the ischemic cortex in MCAO/R rats was observed by 2,3,5-Triphenyl-Tetrazolium Chloride (TTC) staining (Scale bar = 1 cm) (D) and hematoxylin-eosin (HE) staining (Scale bar = 100 μm) (E). Data are signified as the mean ± SEM. **** $p < 0.0001$, *** $p < 0.001$, ** $p < 0.01$ vs. the sham group; $^{\#}$ $p < 0.05$, $^{\#\#\#\#}$ $p < 0.0001$ vs. the model group. ALT, alanine aminotransferase; AST, aspartate aminotransferase; BUN, blood urea nitrogen; Cr, creatinine.

2.20 Snap25 Overexpression in PC12 Cells

Snap25 overexpression plasmids were prepared by Hanbio Corporation (JY20220811WY-PC01). The pcDNA3.1-cytomegalovirus (CMV)-Snap25 plasmids were introduced into PC12 cells via Lipofectamine™ 3000 (L3000015, Invitrogen). A transfection of 1×10^5 PC12 cells was conducted with 10 μg of the Snap25 overexpression plasmid. For the NC group, a transfection of 1×10^5 PC12 cells was conducted with 10 μg of the empty pcDNA3.1-CMV plasmid. The PC12 cells were transfected for 24-h prior to further experiments.

2.21 Statistical Analyses

SPSS software (v 20.0) (IBM Corp., Armonk, NY, USA) was employed for the statistical analysis of data. GraphPad Prism (v 8.0, GraphPad Software, Inc., San Diego, CA, USA) was utilized to create all graphical images. The Kruskal-Wallis non-parametric test or one-way ANOVA compares two or more groups, and then post-hoc analysis with Tukey's multiple comparisons test was conducted. A p-value of <0.05 is significant.

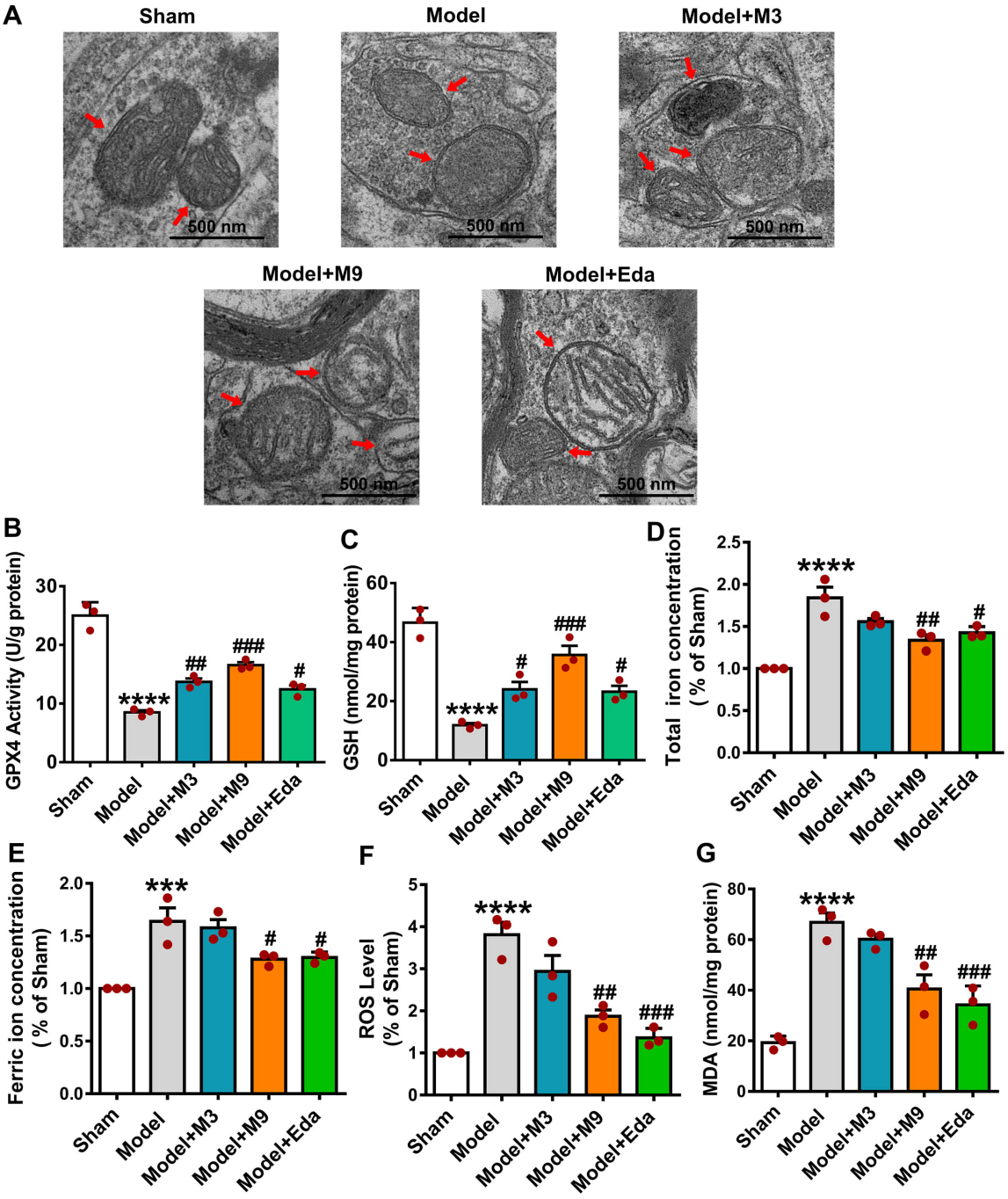

Fig. 2. Muscone attenuates ferroptosis in the ischemic cortex of MCAO/R rats. (A) Transmission electron microscopy (TEM) shows reduced mitochondrial damage in the cortex after muscone treatment. The red arrows indicate mitochondria. Muscone increased glutathione peroxidase 4 (GPX4) activity (B) and glutathione (GSH) levels (C), and decreased total iron (D), ferric iron (E), reactive oxygen species (ROS) (F), and malondialdehyde (MDA) concentrations (G) in MCAO/R rats. Mean ± SEM represents the data; one-way ANOVA. $^{****}p < 0.0001$, $^{***}p < 0.001$, vs. sham; $^{###}p < 0.001$, $^{##}p < 0.01$, $^{#}p < 0.05$ vs. model. Scale bar: 500 nm.

3. Results

3.1 Muscone Mitigates Acute Cerebral Ischemic Injury in MCAO/R Rats

To select the appropriate dose of muscone for experimentation, the liver and kidney functions in rats were first evaluated by serum biochemical indicators. Liver and kidney functions showed no significant damage in the M3 and M9 groups, but substantial liver and kidney toxicity were found in the M18 group, as shown in Fig. 1A (ALT: M18 vs. sham, $p < 0.01$; AST: M18 vs. sham, $p < 0.001$) and Fig. 1B (BUN: M18 vs. sham, $p < 0.01$; Cr: M18 vs. sham, $p < 0.01$). Therefore, concentrations of 3 and 9 mg/kg were

chosen for the next trials. Edaravone (3 mg/kg) was chosen as a positive control since it has been reported to ameliorate damage in MCAO/R rats [37,38]. Neurological deficit scores and infarct volumes were significantly lessened in the M9 and Eda groups compared to the model group, as shown in Fig. 1C ($p < 0.05$) and Fig. 1D ($p < 0.0001$), respectively. HE staining revealed the cortical tissue space in the model group was loose, with unclear tissue structure. In contrast, cortical structures in the M3, M9 and Eda groups exhibited marked improvement (Fig. 1E). Collectively, these outcomes indicate that muscone exerts neuroprotective effects on the brain tissue of rats subjected to MCAO/R damage.

3.2 Muscone Attenuates Ferroptosis in the Ischemic Cortex of MCAO/R Rats

TEM illustrated the disrupted mitochondrial cristae and membranes in the cortical tissue of model rats, which were markedly preserved in the M3, M9, and Eda groups (Fig. 2A). GPX4 activity (Fig. 2B) and GSH levels (Fig. 2C) were significantly higher in these groups vs. the model (M3: $p < 0.01$, $p < 0.05$; M9: $p < 0.001$, $p < 0.001$; Eda: $p < 0.05$, $p < 0.05$). Total iron (Fig. 2D), ferric iron (Fig. 2E), ROS (Fig. 2F), and MDA levels (Fig. 2G) were significantly lower in the M9 and Eda groups vs. the model (M9: $p < 0.01$, $p < 0.05$, $p < 0.01$, $p < 0.01$; Eda: $p < 0.05$, $p < 0.05$, $p < 0.001$, $p < 0.001$). These results indicate that muscone effectively mitigates ferroptosis in the ischemic cortex of MCAO/R-injured rats.

3.3 Downregulated Snap25 Expression in the Ischemic Cortical Tissue of MCAO/R Rats

Cortical tissues from the sham and model groups (n = 3 per group) were subjected to RNA sequencing. DEGs were subsequently identified and analyzed using bioinformatics approaches. The results of GO analysis revealed that Snap25 was significantly enriched in multiple signaling pathways associated with BP (Fig. 3A), CC (Fig. 3B), and MF (Fig. 3C). These results suggest that differential expression of Snap25 may have a crucial function in cortical damage in MCAO/R rats. Heatmaps (Fig. 3D) show a significant downregulation of Snap25 expression in the model group compared to the sham group. WB results shown in Fig. 3E confirm that Snap25 protein expression in the cortex illustrated a significant decrease in the model group (sham vs. model, $p < 0.001$), but increased significantly following administration of muscone (M9 vs. model, $p < 0.05$). These outcomes establish that Snap25 expression decreased significantly under AIS damage-like circumstances, and that administration of muscone could significantly increase Snap25 expression.

3.4 Muscone Reduces the Death of PC12 Cells Subjected to OGD/R Damage

The impact of muscone on PC12 cells exposed to OGD/R was examined using CCK8 assay and live/dead cell staining. CCK8 analysis revealed the M300 group (300 ng/mL muscone) had substantially better cell viability compared to the control group (Fig. 4A; control vs. M300, $p < 0.01$). In contrast, the M600 (600 ng/mL muscone) and M1200 (1200 ng/mL muscone) groups showed markedly reduced cell viability relative to the control group (Fig. 4A; control vs. M600, $p < 0.05$; control vs. M1200, $p < 0.05$). Fig. 4B shows that OGD/R damage caused a significant lessening in PC12 cell viability (control vs. model, $p < 0.0001$). The M100, M300, and ferrostatin-1 (Fer-1) groups showed significantly higher cell viability than the model group (Fig. 4B; $p < 0.05$, $p < 0.001$, and $p < 0.0001$, respectively). Cell death rates were also significantly lower in the M300 and Fer-1 groups (Fig. 4C; both $p < 0.001$ vs. model). Collectively, these outcomes suggest that muscone exerts a substantial protective effect on PC12 cells that have been subjected to OGD/R-induced damage.

3.5 Muscone Decreases Ferroptosis in PC12 Cells Exposed to OGD/R

TEM analysis revealed substantial mitochondrial damage in the model group, such as decreased cristae and disrupted membranes (Fig. 5A). Damage was significantly reduced in the M300 and Fer-1 groups. GPX4 activity (Fig. 5B) and GSH levels (Fig. 5C) were significantly higher in the M100, M300, and Fer-1 groups vs. the model (M100: $p < 0.01$; M300: $p < 0.0001$, $p < 0.001$; Fer-1: $p < 0.05$, $p < 0.01$). Total iron (Fig. 5D), ferrous iron (Fig. 5E), ROS (Fig. 5F), and MDA (Fig. 5G) levels were significantly lower in M300 and Fer-1 groups (M300: $p < 0.01$, $p < 0.05$, $p < 0.01$, $p < 0.01$; Fer-1: $p < 0.05$, $p < 0.05$, $p < 0.001$, $p < 0.001$). Western blot (Fig. 5H) showed Snap25 downregulation in the model group ($p < 0.001$), which was restored in M300 and Fer-1 groups (both $p < 0.05$). These findings indicate muscone alleviates ferroptosis in OGD/R-damaged PC12 cells and enhances Snap25 expression.

3.6 Silencing of Snap25 Expression Increases Ferroptosis and Eliminates the Anti-ferroptosis Impact of Muscone in PC12 Cells Damaged by OGD/R

We next investigated the Snap25 function in the ferroptosis pathway during OGD/R injury by using Snap25-specific siRNAs and NC siRNA. WB results established effective silencing of Snap25 in the *Snap25*-siRNA-1 group compared to the NC group (Fig. 6A; *Snap25*-siRNA-1 vs. NC, $p < 0.0001$). Compared to the NC group, both the *Snap25*-si and *Snap25*-si+muscone groups exhibited significant decreases in Snap25 expression (Fig. 6B; *Snap25*-si vs. NC, $p < 0.05$; *Snap25*-si+muscone vs. NC, $p < 0.05$), GPX4 activity (Fig. 6C; $p < 0.001$, $p < 0.01$), GSH level

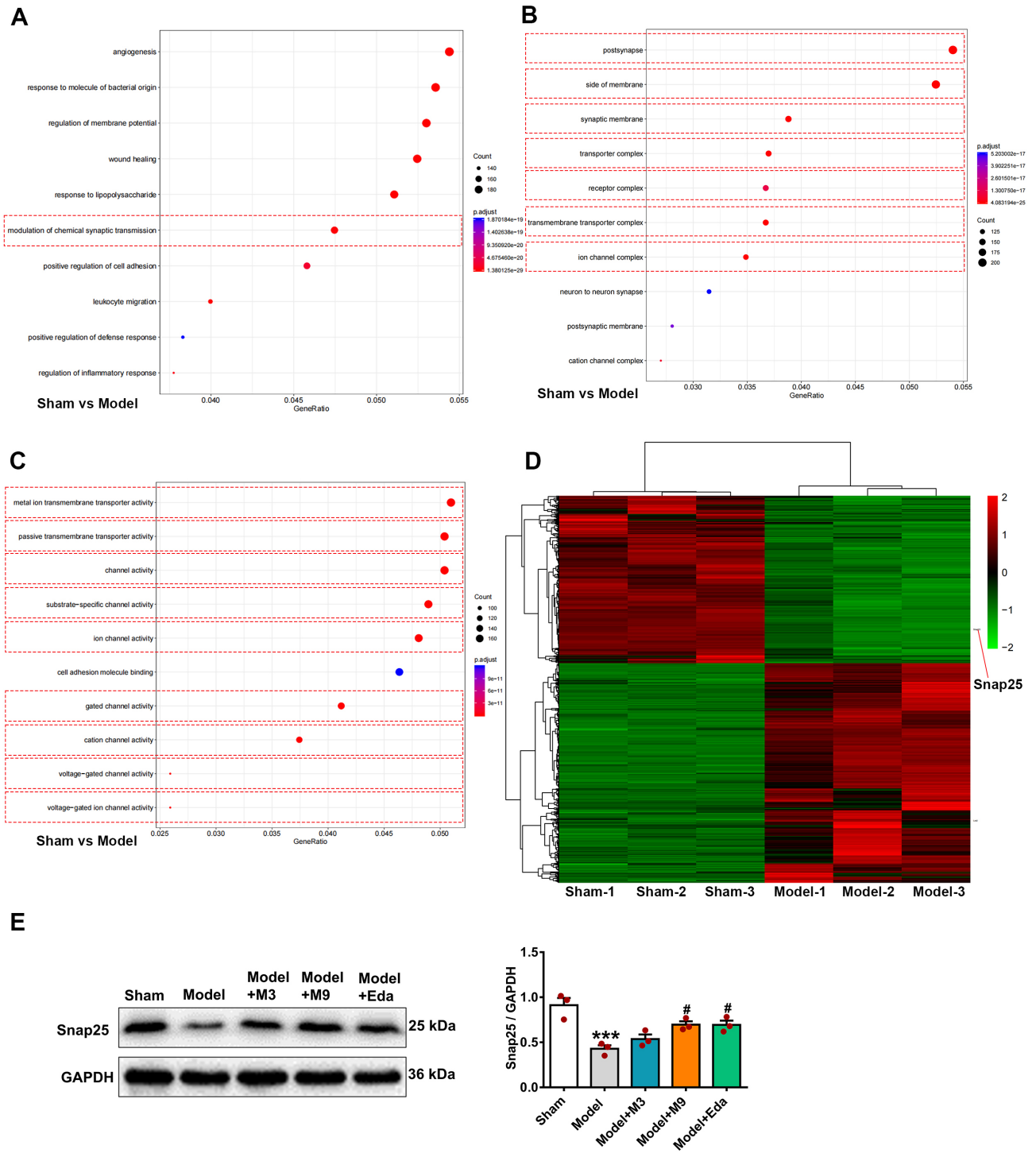

Fig. 3. Decreased Synaptosome-associated protein 25 kDa (Snap25) expression in the ischemic cortical tissue of MCAO/R rats. Cortical tissues from the sham and model groups (n = 3 per group) underwent RNA sequencing to identify differentially expressed genes (DEGs). These were subsequently analyzed using Gene Ontology (GO) enrichment analysis, with the *Snap25* gene found to be prominently involved in several signaling pathways associated with biological process (BP)s (A), cellular component (CC)s (B), and molecular function (MF)s (C). Heatmap visualization (D) revealed a noticeable reduction in *Snap25* expression in the model group relative to the sham group. Additionally, western blotting (WB) analysis (E) revealed that the Snap25 protein level in the rat cortex showed a significant lessening in the model group compared to the sham group, but elevated markedly following muscone treatment. One-way ANOVA compared the means of several groups. Data are shown as the mean ± SEM. *** $p < 0.001$ vs. sham group; # $p < 0.05$ vs. model group.

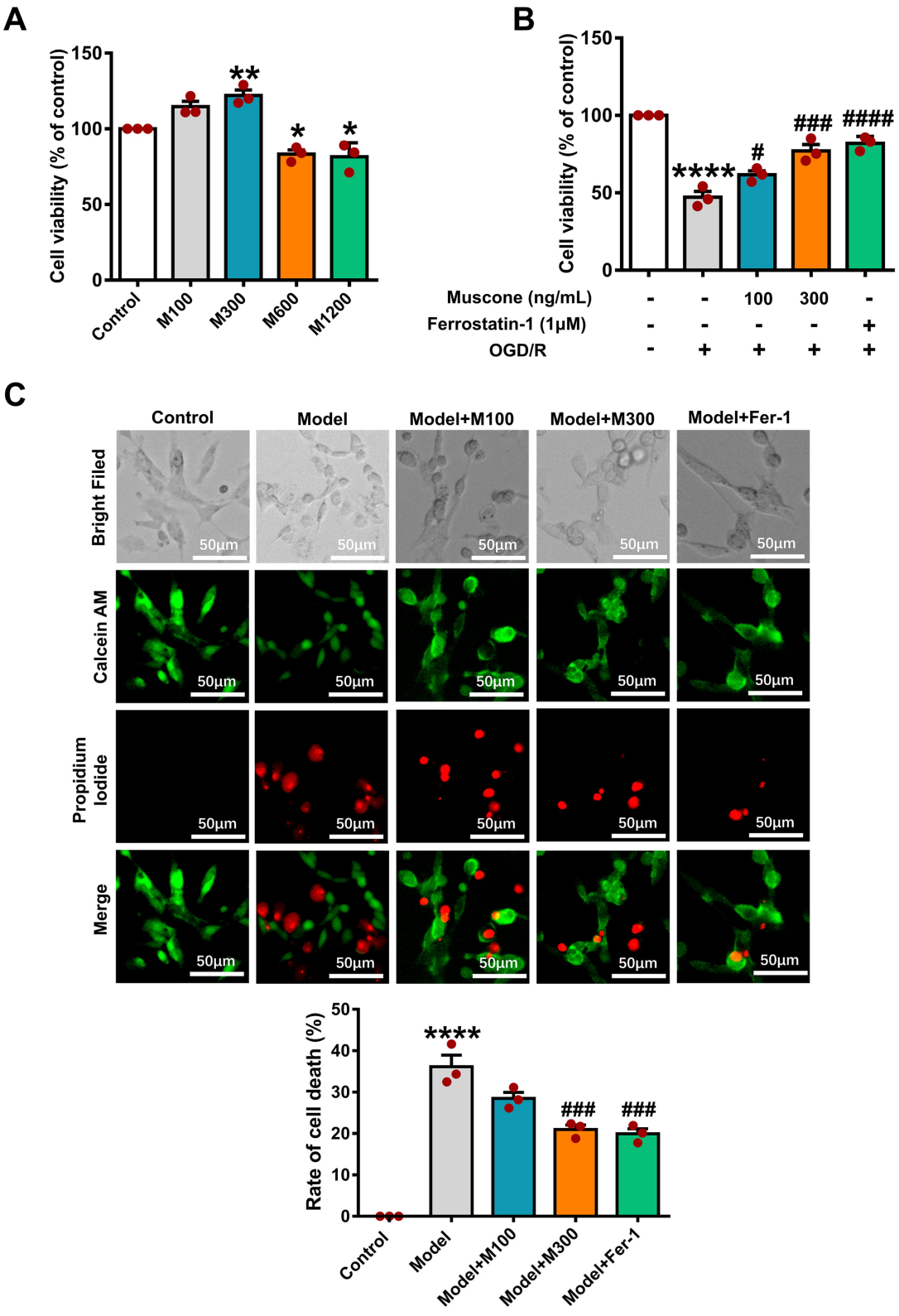

Fig. 4. Muscone reduces mortality in PC12 cells following oxygen-glucose deprivation/reperfusion (OGD/R) damage. (A) CCK-8 assay shows the effects of muscone (100–1200 ng/mL) on PC12 cell viability. (B) Muscone increased viability in OGD/R-injured cells; Ferrostatin-1 served as a positive control. (C) Live/dead staining indicates muscone (100 and 300 ng/mL) reduced cell mortality after OGD/R. Data are mean ± SEM; one-way ANOVA. $^{****}p < 0.0001$, $^{**}p < 0.01$, $^{*}p < 0.05$ vs. control; $^{\#\#\#\#}p < 0.0001$, $^{\#\#\#}p < 0.001$, $^{\#}p < 0.05$ vs. model. Scale bar: 50 μm.

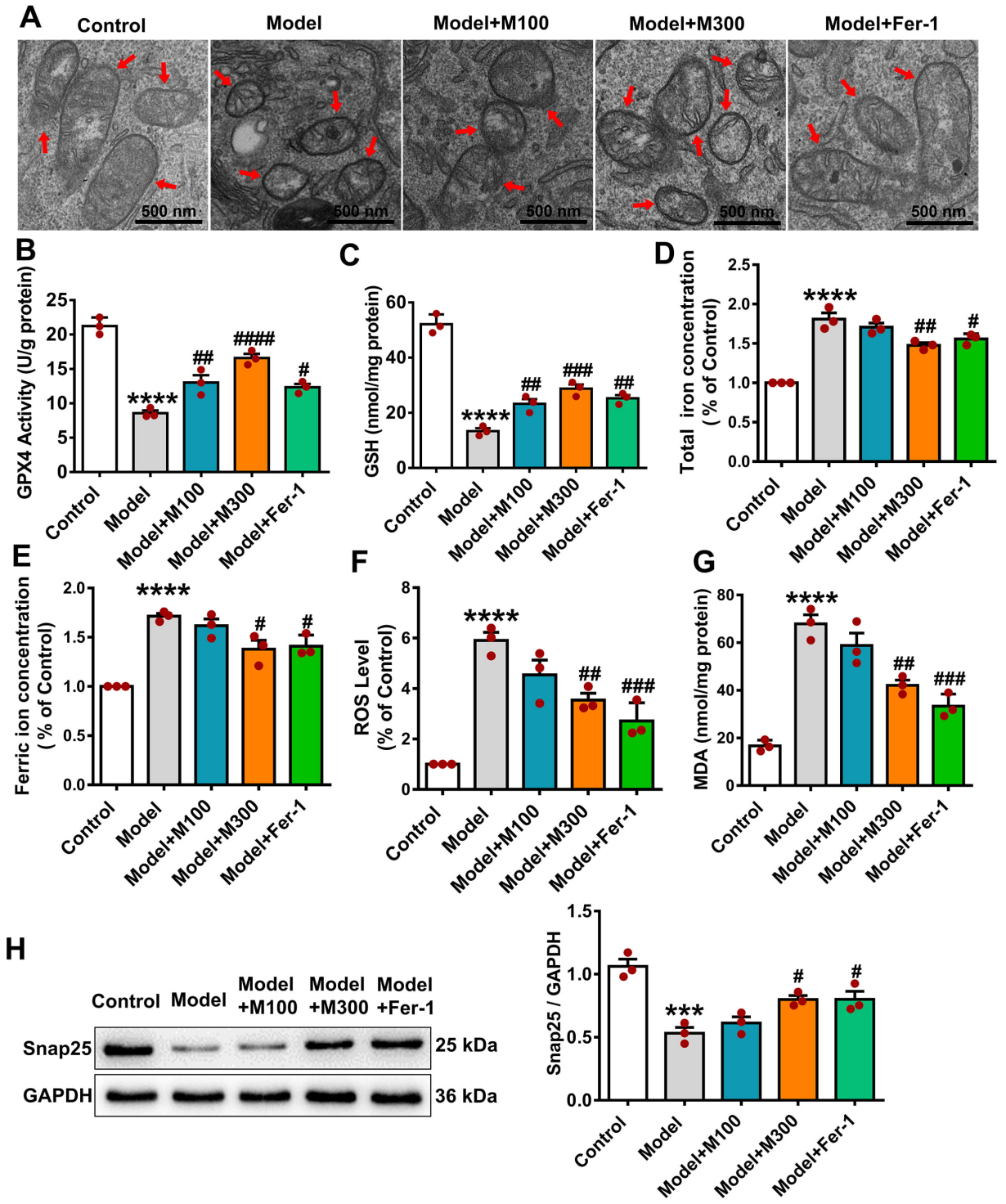

Fig. 5. Muscone decreases ferroptosis in PC12 cells exposed to OGD/R. (A) Muscone attenuates mitochondrial damage in OGD/R-injured PC12 cells. The red arrows indicate mitochondria. Scale bar: 500 nm. Muscone increased GPX4 activity (B) and GSH levels (C), while decreasing total iron (D), ferric iron (E), ROS (F), and MDA levels (G). (H) Snap25 protein expression, reduced by OGD/R, was restored by muscone. Data are mean ± SEM; one-way ANOVA. $^{****}p < 0.0001$, $^{***}p < 0.001$ vs. control; $^{\#}p < 0.05$, $^{\#\#}p < 0.01$, $^{\#\#\#}p < 0.001$, $^{\#\#\#\#}p < 0.0001$ vs. model.

(Fig. 6D; $p < 0.01$, $p < 0.05$), and cell viability (Fig. 6G; $p < 0.05$, $p < 0.01$). Significant increases in the levels of ROS (Fig. 6E; $p < 0.01$, $p < 0.01$) and MDA (Fig. 6F; $p < 0.01$, $p < 0.05$) were observed in the *Snap25*-si and *Snap25*-si+muscone groups, respectively, compared to the NC group. Representative TEM images showed more se-

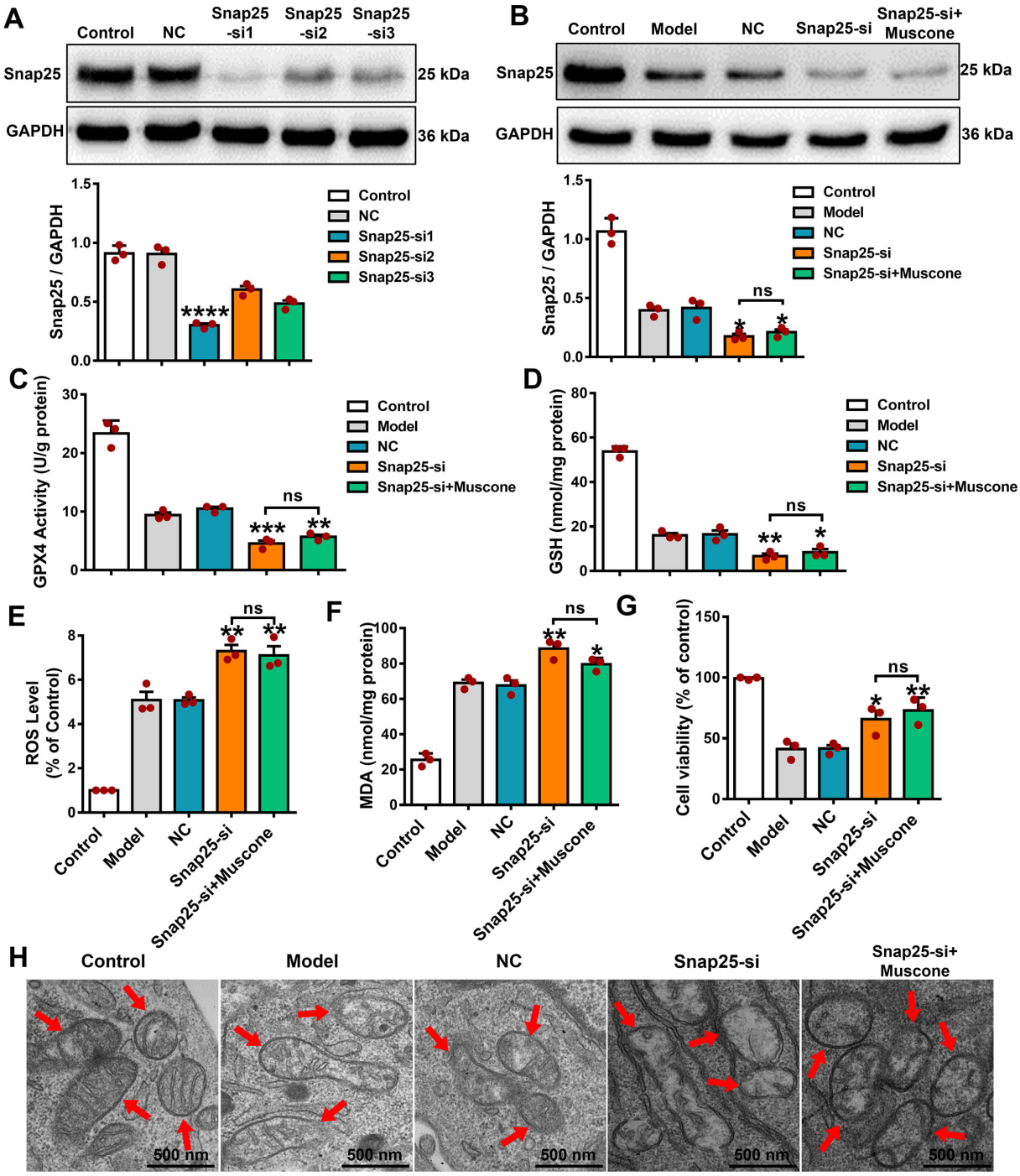

Fig. 6. Snap25 silencing increased the level of ferroptosis and eliminated the anti-ferroptosis impact of muscone in OGD/R-damaged PC12 cells. (A) Effective knockdown of Snap25 in PC12 cells. WB analysis established the effective reduction of Snap25 expression in PC12 cells. (B) Snap25 expression following knockdown and muscone treatment of PC12 cells exposed to OGD/R. GPX4 activity (C) and GSH (D) levels after Snap25 knockdown and muscone administration in OGD/R-injured PC12 cells. In addition, the ROS (E), MDA levels (F), and cell viability (G) were assessed after Snap25 silencing and muscone treatment in PC12 cells subjected to OGD/R injury. (H) Representative TEM images after Snap25 silencing and muscone treatment of PC12 cells exposed to OGD/R. The red arrows indicate mitochondria. Scale bar, 500 nm. One-way ANOVA compares the means of multiple groups. Data shown are the mean ± SEM. **** $p < 0.0001$, *** $p < 0.001$, ** $p < 0.01$, * $p < 0.05$ vs. the negative control (NC) group; ns, no statistical significance, *Snap25*-si group vs. *Snap25*-si+muscone group.

vere ultrastructural damage of mitochondrial crista in the *Snap25*-si and *Snap25*-si+muscone groups compared to the model group (Fig. 6H). Notably, the level of damage between the *Snap25*-si and *Snap25*-si+muscone groups was not statistically different. These results indicate that silencing of Snap25 expression increases the ferroptosis level in OGD/R-injured PC12 cells. Moreover, Snap25 silencing eliminated the anti-ferroptosis impact of muscone in OGD/R-injured PC12 cells, thereby demonstrating target specificity for the interaction between muscone and Snap25 protein.

3.7 Overexpression of Snap25 Reduces the Ferroptosis Level and Strengthens the Anti-ferroptosis Effects of Muscone in OGD/R-damaged PC12 Cells

WB analysis established the effective Snap25 upregulation in the *Snap25*-over expression (OE) group in comparison to the NC group (Fig. 7A; $p < 0.01$). When compared to the NC group, both the *Snap25*-OE and *Snap25*-OE+muscone groups showed significant increases in Snap25 expression (Fig. 7B: *Snap25*-OE vs. NC, $p < 0.05$; *Snap25*-OE+muscone vs. NC, $p < 0.001$), GPX4 activity (Fig. 7C: $p < 0.01$, $p < 0.0001$), GSH level (Fig. 7D: $p < 0.001$, $p < 0.0001$), and cell viability (Fig. 7G: $p < 0.05$, $p < 0.001$). Additionally, marked decreases in ROS (Fig. 7E: $p < 0.01$, $p < 0.0001$) and MDA levels (Fig. 7F: $p < 0.0001$, $p < 0.0001$) were observed in the *Snap25*-OE and *Snap25*-OE+muscone groups. TEM images showed significantly improved mitochondrial cristae ultrastructure in the *Snap25*-OE and *Snap25*-OE+muscone groups compared to the model group (Fig. 7H). Compared to the *Snap25*-OE group, the *Snap25*-OE+muscone group showed substantially higher levels of Snap25 protein expression (Fig. 7B: $p < 0.05$), GPX4 activity (Fig. 7C: $p < 0.05$), GSH concentration (Fig. 7D: $p < 0.01$), and cell viability (Fig. 7G: $p < 0.05$), but notable reductions in ROS (Fig. 7E: $p < 0.05$) and MDA (Fig. 7F: $p < 0.05$) levels. Additionally, the mitochondrial ultrastructure exhibited significant improvement in the *Snap25*-OE+muscone group (Fig. 7H). Together, these outcomes indicate that Snap25 overexpression mitigates ferroptosis and enhances the protective effect of muscone against ferroptosis in OGD/R-injured PC12 cells, thus highlighting the specific interaction between muscone and the Snap25 protein.

3.8 Muscone Binds to Snap25 Protein and Enhances its Structural Stability

Molecular docking experiments predicted the binding sites of muscone and Snap25. This revealed 8 potential amino acid residues (Ser-25, Ser-28, Thr-29, Met-32, Ile-129, Phe-133, and Ile-134) involved in the interaction between muscone and Snap25 protein (Fig. 8A, $\Delta G = -6.5$ kcal/mol). The results of SPR technology revealed a significant and direct binding effect between muscone and Snap25 protein (Fig. 8B, $K_D = 7.14 \times 10^{-6}$; Ka = 5.81×10^{4}; Kd = 4.15×10^{-1}), thus confirming the results of the molecular docking experiments. MD simulations were subsequently carried out to assess the effect of muscone binding on the structural dynamics of Snap25. Analysis of root mean square deviation (RMSD), root mean square fluctuation (RMSF) and radius of gyration (Rg) revealed that binding of muscone enhanced the stability (Fig. 8C), reduced the flexibility (Fig. 8D), and increased the overall structural compactness (Fig. 8E) of Snap25 protein. Solvent accessible surface area (SASA) analysis found that binding of muscone reduced the overall solvent-accessible surface area of the Snap25 protein (Fig. 8F). Hydrogen bond analysis revealed that binding of muscone to the Snap25 protein exerted a protective effect on the stability of the internal hydrogen bond network (Fig. 8G). The Gibbs free energy analysis revealed that binding of muscone resulted in a more concentrated distribution of free energy and promoted a more stable conformational state (Fig. 8H). Visualization analysis of protein structure showed that binding of muscone strongly maintained the overall conformation of the Snap25 protein (Fig. 8I). These findings indicate the interaction between muscone and Snap25 is characterized by a moderate level of free energy and strong binding stability, thereby enhancing the structural stability and compactness of the Snap25 protein.

4. Discussion

The multifaceted pathogenesis of AIS means the therapeutic window is narrow, resulting in severely compromised neurological function. Drug therapy for AIS has so far failed to produce satisfactory clinical outcomes. Therefore, it is important to elucidate the specific pathogenic mechanism of AIS to facilitate the development of effective drugs. The key findings of this investigation can be summarized as follows: (1) markedly elevated ferroptosis levels were observed in both the MCAO/R model and OGD/R-treated PC12 cells; (2) muscone significantly alleviated AIS-triggered damage both *in vivo* and *in vitro* by effectively decreasing ferroptosis levels; (3) binding of muscone to the Snap25 protein enhances its expression and structural stability, thereby reducing the ferroptosis level in AIS damage.

The role of ferroptosis in stroke pathology has recently gained significant attention. Multiple studies have suggested that AIS is closely related to ferroptosis [39–41]. AIS-damaged rat models with excessive iron intake were found to have severe neuronal damage. Moreover, iron chelating agents can decrease reperfusion damage in AIS animal models, suggesting that neuron injury in AIS may be closely related to iron accumulation [42]. An excessive increase in the ROS level is the main cause of ferroptosis [43]. Intracellular lipid molecules, such as cell membranes, are the main target affinity of ROS [44]. Therefore, excessive ROS levels result in a higher level of lipid peroxidation [45,46]. Herein, we detected substantial increases

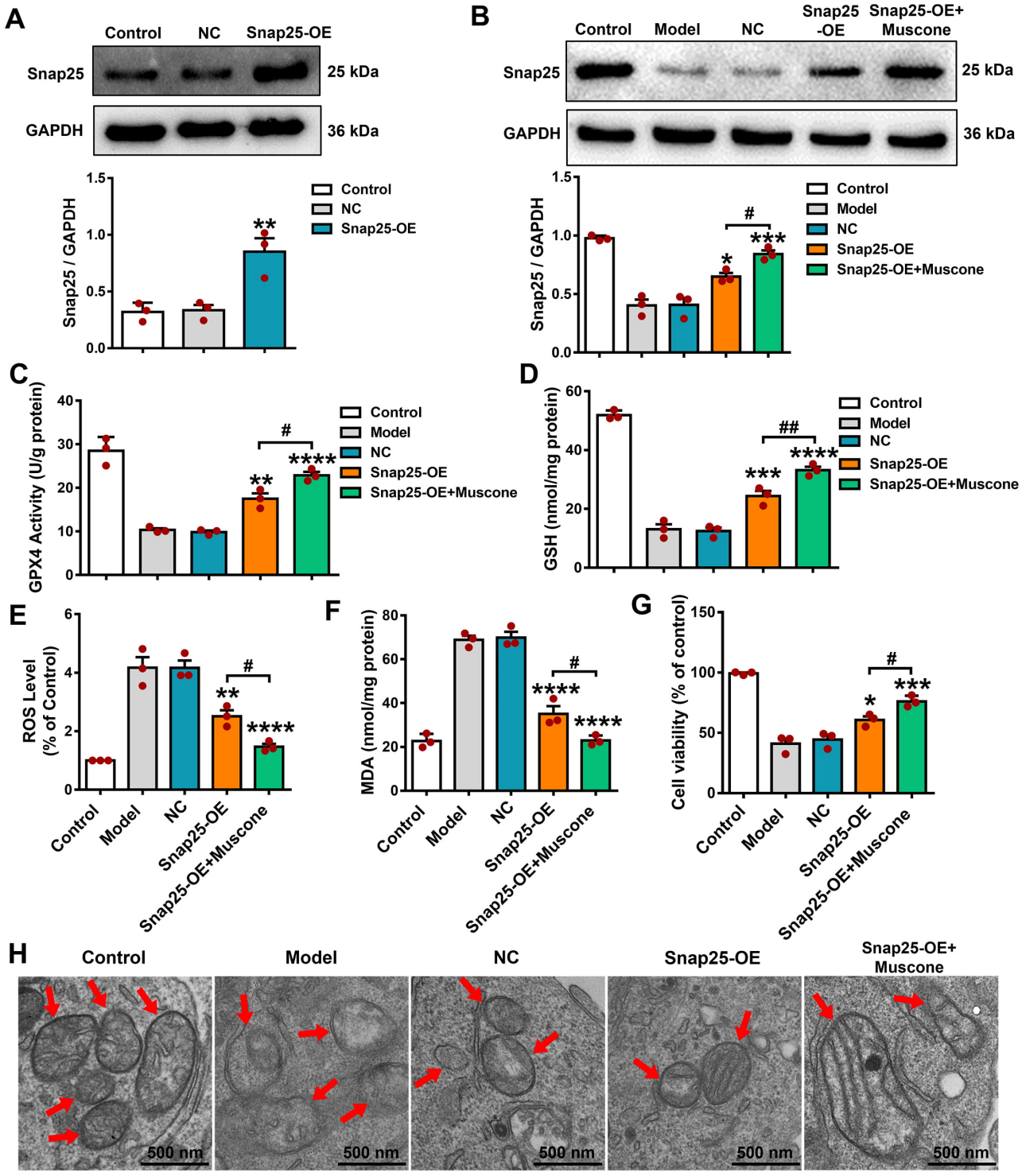

Fig. 7. Overexpression of Snap25 reduced the ferroptosis level and strengthened the anti-ferroptosis effects of muscone in OGD/R-injured PC12 cells. (A) WB analysis confirmed the Snap25 overexpression in PC12 cells. (B) Following Snap25 overexpression and muscone administration in PC12 cells exposed to OGD/R damage, significant increases were observed in GPX4 activity (C) and GSH levels (D). Furthermore, Snap25 overexpression combined with muscone treatment led to decreases in ROS (E) and MDA levels (F), increased cell viability (G), and attenuation of mitochondrial injury (H) in PC12 cells subjected to OGD/R. The red arrows indicate mitochondria. Scale bar, 500 nm. One-way ANOVA compared the means of multiple groups. Data shown are the mean ± SEM. **** $p < 0.0001$, *** $p < 0.001$, ** $p < 0.01$, * $p < 0.05$ vs. NC group; $^{\#\#}$ $p < 0.01$, $^{\#}$ $p < 0.05$, *Snap25*- over expression (OE) group vs. *Snap25*-OE+muscone group.

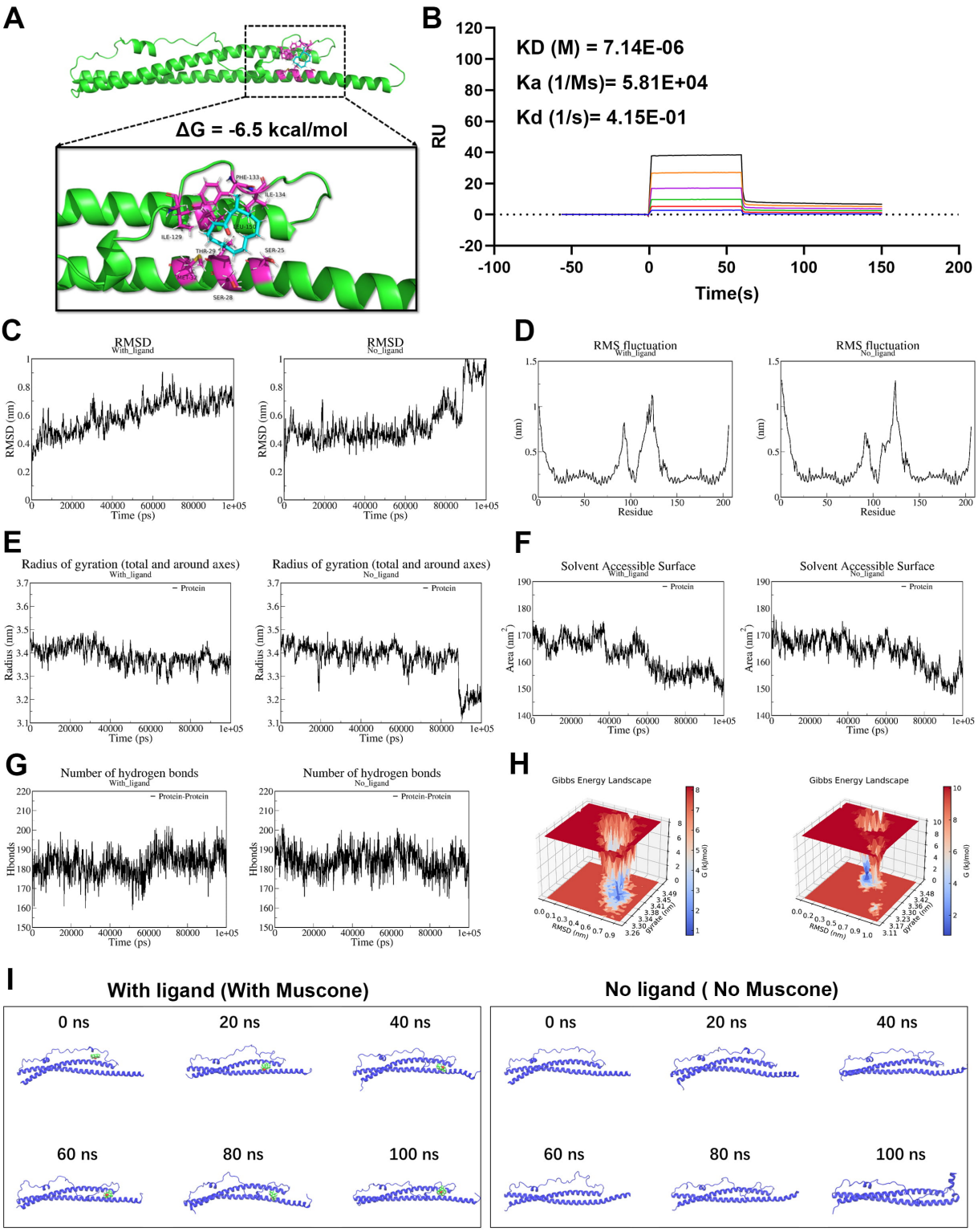

Fig. 8. Muscone binds to Snap25 protein and enhances its structural stability. Molecular docking tests were conducted to predict the binding sites between muscone and Snap25. (A) Stereoview of the binding mode for Snap25 with muscone. (B) Surface plasmon resonance (SPR) analysis showing the direct binding effect between muscone and Snap25 protein (K_D = 7.14 × 10^{-6}; Ka = 5.81 × 10^4; Kd = 4.15 × 10^{-1}). Analysis of the root mean square deviation (RMSD) (C), root mean square fluctuation (RMSF) (D), radius of gyration (E), solvent accessible surface area (SASA) (F), hydrogen bond analysis (G), Gibbs free energy (H), and visualization analysis of the protein structure (I). Together, these analyses revealed that binding of muscone to Snap25 is characterized by moderate free energy and robust binding stability, thus significantly enhancing the structural stability and compactness of the Snap25 protein.

in ROS and lipid peroxidation levels, as well as significant mitochondrial ridge breakage, in *in vivo* and *in vitro* AIS models. These findings further confirm the pivotal participation of ferroptosis in the pathological progression of AIS and offer a mechanistic foundation for potential therapeutic interventions that target AIS injury.

For centuries, the TCM compound musk has been employed in treating stroke injuries. The potential anti-stroke properties of muscone, the principal active constituent of musk, have been widely recognized. Muscone is a small active molecule that can enter the blood-brain barrier and exert neuroprotective effects. Previous studies have suggested that muscone may be protective against AIS injury by promoting microglia polarization or by inhibiting cell apoptosis [47,48]. Herein, we detected a significant reduction in infarct volume following muscone treatment of MCAO/R rats, as well as increased survival of OGD/R cells. Furthermore, muscone treatment in the AIS model resulted in notable improvements in mitochondrial morphology, increased GPX4 activity and GSH level, and decreased ROS and MDA levels, thus indicating an anti-ferroptosis effect. However, the precise mechanism by which muscone regulates ferroptosis in AIS remains unclear. Snap25 has an essential function in various neurological diseases and pathological conditions, and is significantly correlated with AIS injury. Research has demonstrated that Snap25 expression in mouse models of ischemic stroke is significantly decreased in the injured brain tissue. However, upon expression of Snap25 there is marked improvement in the synaptic structure of ischemia-injured neurons [49]. RNA sequencing and bioinformatics analysis in this investigation revealed a noticeable decrease in Snap25 expression in the *in vitro* and *in vivo* AIS models, thus corroborating previous findings. A deficiency in Snap25 leads to neurotransmitter transmission disorders, increased ROS levels, and neuroinflammation, which may be key factors in Snap25-induced ferroptosis [50]. Our previous studies and current research indicate that Snap25 regulates the level of ferroptosis in AIS. Through a series of experiments, including Snap25 silencing and overexpression, this investigation detected Snap25 as a target of muscone. Specifically, muscone mitigated ferroptosis during AIS injury by upregulating the expression of Snap25 protein. We conducted molecular docking, SPR detection, and MD simulation experiments to illuminate the mechanism by which muscone increases the Snap25 protein expression. These revealed multiple potential binding sites and a direct binding effect between muscone and the Snap25 protein. Moreover, muscone can significantly enhance the structural stability of Snap25 and prevent its degradation under conditions of AIS injury. Our results provide a molecular basis for the substantial upregulation of Snap25 expression following muscone treatment, leading to mitigation of ferroptosis injury in AIS.

This research study has certain limitations. Although we examined the mechanism by which muscone controls the expression and stability of Snap25 protein and protects against ferroptosis-induced injury through *in vitro* silencing and overexpression experiments, further *in vivo* validation experiments are necessary. In subsequent studies, we intend to utilize adeno-associated, virus-mediated infection techniques to conduct Snap25 silencing and overexpression experiments at the animal level, thereby further confirming the specific interaction between muscone and Snap25 protein. Future research should also investigate the therapeutic potential of muscone in various subtypes of ischemic stroke injuries, including its capacity to alleviate small deep brain infarctions associated with lacunar syndrome [51].

5. Conclusion

This study confirmed the correlation between AIS and ferroptosis, while specifically investigating the protective mechanism of muscone in AIS. Our research findings indicate that muscone can attenuate ferroptosis during AIS injury by increasing the expression of Snap25. Consequently, this research provides additional evidence supporting a close association between AIS injury and ferroptosis. This could potentially lead to the development of more effective therapeutic medications for clinical application in AIS.

Availability of Data and Materials

Datasets generated for this study are available upon request from the corresponding author.

Author Contributions

RJY conducted the animal and cell experiments and drafted the manuscript. BS and JL performed the animal and cell experiments and analyzed the experimental data. GHH carried out the GSH and GPX4 activity analyses. NS conducted the ROS and CCK-8 assays. BS, JL, GHH and NS revised the manuscript critically for important intellectual content. WWS performed molecular docking and molecular dynamics simulations, provided technical guidance on the experiments, and reviewed and edited the manuscript. All authors have read and approved the final version of the manuscript. All authors have participated sufficiently in the work and agreed to be accountable for all aspects of the work.

Ethics Approval and Consent to Participate

The Ethical Committee of Animal Experiments of the Anhui University of Chinese Medicine (Hefei, China; approval no. AHUCM-rats-2023126) specifically approved animal experiments. The study was carried out in compliance with ARRIVE guidelines.

Acknowledgment

Not applicable.

Funding

This research was supported by the National Natural Science Foundation of China (grant no. 82374209 and 82104570), the Anhui Provincial Natural Science Foundation (grant no. 2208085Y33), the Talent Project of Anhui University of Chinese Medicine (grant no. 2022rczd007), and the Natural Science Research Projects at Higher Institutions in Anhui Province (grant no. 2023AH050748).

Conflict of Interest

The authors declare no conflict of interest.

Supplementary Material

Supplementary material associated with this article can be found, in the online version, at https://doi.org/10.31083/JIN39116.

References

[1] Buch E, Weber C, Cohen LG, Braun C, Dimyan MA, Ard T, *et al*. Think to move: a neuromagnetic brain-computer interface (BCI) system for chronic stroke. Stroke. 2008; 39: 910–917. https://doi.org/10.1161/STROKEAHA.107.505313.

[2] Mason B, Boyd K, Doubal F, Barber M, Brady M, Cowey E, *et al*. Core Outcome Measures for Palliative and End-of-Life Research After Severe Stroke: Mixed-Method Delphi Study. Stroke. 2021; 52: 3507–3513. https://doi.org/10.1161/STROKEAHA.120.032650.

[3] Wu H, Peng B, Mohammed FS, Gao X, Qin Z, Sheth KN, *et al*. Brain Targeting, Antioxidant Polymeric Nanoparticles for Stroke Drug Delivery and Therapy. Small (Weinheim an Der Bergstrasse, Germany). 2022; 18: e2107126. https://doi.org/10.1002/smll.202107126.

[4] Mazuryk J, Puchalska I, Koziński K, Ślusarz MJ, Ruczyński J, Rekowski P, *et al*. PTD4 Peptide Increases Neural Viability in an In Vitro Model of Acute Ischemic Stroke. International Journal of Molecular Sciences. 2021; 22: 6086. https://doi.org/10.3390/ijms22116086.

[5] Pan A, Sun Q, Okereke OI, Rexrode KM, Hu FB. Depression and risk of stroke morbidity and mortality: a meta-analysis and systematic review. JAMA. 2011; 306: 1241–1249. https://doi.org/10.1001/jama.2011.1282.

[6] Pan B, Sun J, Liu Z, Wang L, Huo H, Zhao Y, *et al*. *Longxuetongluo Capsule* protects against cerebral ischemia/reperfusion injury through endoplasmic reticulum stress and MAPK-mediated mechanisms. Journal of Advanced Research. 2021; 33: 215–225. https://doi.org/10.1016/j.jare.2021.01.016.

[7] Lyden S, Wold J. Acute Treatment of Ischemic Stroke. Neurologic Clinics. 2022; 40: 17–32. https://doi.org/10.1016/j.ncl.2021.08.002.

[8] Mendelson SJ, Prabhakaran S. Diagnosis and Management of Transient Ischemic Attack and Acute Ischemic Stroke: A Review. JAMA. 2021; 325: 1088–1098. https://doi.org/10.1001/jama.2020.26867.

[9] Robba C, van Dijk EJ, van der Jagt M. Acute ischaemic stroke and its challenges for the intensivist. European Heart Journal. Acute Cardiovascular Care. 2022; 11: 258–268. https://doi.org/10.1093/ehjacc/zuac004.

[10] Jolugbo P, Ariëns RAS. Thrombus Composition and Efficacy of Thrombolysis and Thrombectomy in Acute Ischemic Stroke. Stroke. 2021; 52: 1131–1142. https://doi.org/10.1161/STROKEAHA.120.032810.

[11] Tan YF, Zhan LX, Chen XH, Guo JJ, Qin C, Xu E. Risk Factors, Clinical Features and Prognosis for Subtypes of Ischemic Stroke in a Chinese Population. Current Medical Science. 2018; 38: 296–303. https://doi.org/10.1007/s11596-018-1878-1.

[12] Finn C, Hung P, Patel P, Gupta A, Kamel H. Relationship Between Visceral Infarction and Ischemic Stroke Subtype. Stroke. 2018; 49: 727–729. https://doi.org/10.1161/STROKEAHA.117.020035.

[13] Kim BJ, Kim JS. Ischemic stroke subtype classification: an asian viewpoint. Journal of Stroke. 2014; 16: 8–17. https://doi.org/10.5853/jos.2014.16.1.8.

[14] Lu J, Xu F, Lu H. LncRNA PVT1 regulates ferroptosis through miR-214-mediated TFR1 and p53. Life Sciences. 2020; 260: 118305. https://doi.org/10.1016/j.lfs.2020.118305.

[15] Wang SW, Liu Z, Shi ZS. Non-Coding RNA in Acute Ischemic Stroke: Mechanisms, Biomarkers and Therapeutic Targets. Cell Transplantation. 2018; 27: 1763–1777. https://doi.org/10.1177/0963689718806818.

[16] Ma Y, Wang X, Li Y, Zhao J, Zhou X, Wang X. Mechanisms Associated with Mitophagy and Ferroptosis in Cerebral Ischemia-reperfusion Injury. Journal of Integrative Neuroscience. 2025; 24: 26458. https://doi.org/10.31083/JIN26458.

[17] Lapp DW, Zhang SS, Barnstable CJ. Stat3 mediates LIF-induced protection of astrocytes against toxic ROS by upregulating the UPC2 mRNA pool. Glia. 2014; 62: 159–170. https://doi.org/10.1002/glia.22594.

[18] Singhal A, Morris VB, Labhasetwar V, Ghorpade A. Nanoparticle-mediated catalase delivery protects human neurons from oxidative stress. Cell Death & Disease. 2013; 4: e903. https://doi.org/10.1038/cddis.2013.362.

[19] Kim S, Kang IH, Nam JB, Cho Y, Chung DY, Kim SH, *et al*. Ameliorating the effect of astragaloside IV on learning and memory deficit after chronic cerebral hypoperfusion in rats. Molecules (Basel, Switzerland). 2015; 20: 1904–1921. https://doi.org/10.3390/molecules20021904.

[20] Liang D, Minikes AM, Jiang X. Ferroptosis at the intersection of lipid metabolism and cellular signaling. Molecular Cell. 2022; 82: 2215–2227. https://doi.org/10.1016/j.molcel.2022.03.022.

[21] Youssef LA, Rebbaa A, Pampou S, Weisberg SP, Stockwell BR, Hod EA, *et al*. Increased erythrophagocytosis induces ferroptosis in red pulp macrophages in a mouse model of transfusion. Blood. 2018; 131: 2581–2593. https://doi.org/10.1182/blood-2017-12-822619.

[22] Zhang C, Liu X, Jin S, Chen Y, Guo R. Ferroptosis in cancer therapy: a novel approach to reversing drug resistance. Molecular Cancer. 2022; 21: 47. https://doi.org/10.1186/s12943-022-01530-y.

[23] Fang Y, Chen X, Tan Q, Zhou H, Xu J, Gu Q. Inhibiting Ferroptosis through Disrupting the NCOA4-FTH1 Interaction: A New Mechanism of Action. ACS Central Science. 2021; 7: 980–989. https://doi.org/10.1021/acscentsci.0c01592.

[24] Verma N, Vinik Y, Saroha A, Nair NU, Ruppin E, Mills G, *et al*. Synthetic lethal combination targeting BET uncovered intrinsic susceptibility of TNBC to ferroptosis. Science Advances. 2020; 6: eaba8968. https://doi.org/10.1126/sciadv.aba8968.

[25] Chai Z, Zheng J, Shen J. Mechanism of ferroptosis regulating ischemic stroke and pharmacologically inhibiting ferroptosis in treatment of ischemic stroke. CNS Neuroscience & Therapeutics. 2024; 30: e14865. https://doi.org/10.1111/cns.14865.

[26] Sun WY, Tyurin VA, Mikulska-Ruminska K, Shrivastava IH, Anthonymuthu TS, Zhai YJ, *et al*. Phospholipase iPLA$_2\beta$ averts ferroptosis by eliminating a redox lipid death signal. Nature

Chemical Biology. 2021; 17: 465–476. https://doi.org/10.1038/s41589-020-00734-x.

[27] Zhi Y, Gao L, Wang B, Ren W, Liang KX, Zhi K. Ferroptosis Holds Novel Promise in Treatment of Cancer Mediated by Non-coding RNAs. Frontiers in Cell and Developmental Biology. 2021; 9: 686906. https://doi.org/10.3389/fcell.2021.686906.

[28] Wang X, Meng H, Chen P, Yang N, Lu X, Wang ZM, *et al*. Beneficial effects of muscone on cardiac remodeling in a mouse model of myocardial infarction. International Journal of Molecular Medicine. 2014; 34: 103–111. https://doi.org/10.3892/ijmm.2014.1766.

[29] Wei G, Chen DF, Lai XP, Liu DH, Deng RD, Zhou JH, *et al*. Muscone exerts neuroprotection in an experimental model of stroke via inhibition of the fas pathway. Natural Product Communications. 2012; 7: 1069–1074.

[30] Wang Q, Wang Y, Ji W, Zhou G, He K, Li Z, *et al*. SNAP25 is associated with schizophrenia and major depressive disorder in the Han Chinese population. The Journal of Clinical Psychiatry. 2015; 76: e76–82. https://doi.org/10.4088/JCP.13m08962.

[31] Yang Y, Peng G, Zeng H, Fang D, Zhang L, Xu S, *et al*. Effects of the *SNAP25* on Integration Ability of Brain Functions in Children With ADHD. Journal of Attention Disorders. 2022; 26: 88–100. https://doi.org/10.1177/1087054720964561.

[32] Wood H. SNAP25 - an early biomarker in AD and CJD. Nature Reviews. Neurology. 2022; 18: 575. https://doi.org/10.1038/s41582-022-00720-y.

[33] Alten B, Zhou Q, Shin OH, Esquivies L, Lin PY, White KI, *et al*. Role of Aberrant Spontaneous Neurotransmission in SNAP25-Associated Encephalopathies. Neuron. 2021; 109: 59–72.e5. https://doi.org/10.1016/j.neuron.2020.10.012.

[34] Wang W, Gao W, Zhang L, Xia Z, Zhao B. SNAP25 ameliorates postoperative cognitive dysfunction by facilitating PINK1-dependent mitophagy and impeding caspase-3/GSDME-dependent pyroptosis. Experimental Neurology. 2023; 367: 114463. https://doi.org/10.1016/j.expneurol.2023.114463.

[35] Si W, Ye S, Ren Z, Liu X, Wu Z, Li Y, *et al*. miR 335 promotes stress granule formation to inhibit apoptosis by targeting ROCK2 in acute ischemic stroke. International Journal of Molecular Medicine. 2019; 43: 1452–1466. https://doi.org/10.3892/ijmm.2019.4073.

[36] Longa EZ, Weinstein PR, Carlson S, Cummins R. Reversible middle cerebral artery occlusion without craniectomy in rats. Stroke. 1989; 20: 84–91. https://doi.org/10.1161/01.str.20.1.84.

[37] Shi F, He Z, Wang L, Su H, Han S. Cost-effectiveness of edaravone dexborneol versus edaravone for the treatment of acute ischemic stroke in China: Based on the TASTE study. Frontiers in Pharmacology. 2022; 13: 938239. https://doi.org/10.3389/fphar.2022.938239.

[38] Kobayashi S, Fukuma S, Ikenoue T, Fukuhara S, Kobayashi S. Effect of Edaravone on Neurological Symptoms in Real-World Patients With Acute Ischemic Stroke. Stroke. 2019; 50: 1805–1811. https://doi.org/10.1161/STROKEAHA.118.024351.

[39] Wang P, Cui Y, Ren Q, Yan B, Zhao Y, Yu P, *et al*. Mitochondrial ferritin attenuates cerebral ischaemia/reperfusion injury by inhibiting ferroptosis. Cell Death & Disease. 2021; 12: 447. https://doi.org/10.1038/s41419-021-03725-5.

[40] Li C, Sun G, Chen B, Xu L, Ye Y, He J, *et al*. Nuclear receptor coactivator 4-mediated ferritinophagy contributes to cerebral ischemia-induced ferroptosis in ischemic stroke. Pharmacological Research. 2021; 174: 105933. https://doi.org/10.1016/j.phrs.2021.105933.

[41] Xu Y, Li K, Zhao Y, Zhou L, Liu Y, Zhao J. Role of Ferroptosis in Stroke. Cellular and Molecular Neurobiology. 2023; 43: 205–222. https://doi.org/10.1007/s10571-022-01196-6.

[42] Tuo QZ, Lei P. Ferroptosis in ischemic stroke: Animal models and mechanisms. Zoological Research. 2024; 45: 1235–1248. https://doi.org/10.24272/j.issn.2095-8137.2024.239.

[43] Wang B, Wang Y, Zhang J, Hu C, Jiang J, Li Y, *et al*. ROS-induced lipid peroxidation modulates cell death outcome: mechanisms behind apoptosis, autophagy, and ferroptosis. Archives of Toxicology. 2023; 97: 1439–1451. https://doi.org/10.1007/s00204-023-03476-6.

[44] Stockwell BR, Friedmann Angeli JP, Bayir H, Bush AI, Conrad M, Dixon SJ, *et al*. Ferroptosis: A Regulated Cell Death Nexus Linking Metabolism, Redox Biology, and Disease. Cell. 2017; 171: 273–285. https://doi.org/10.1016/j.cell.2017.09.021.

[45] Xu W, Sun T, Wang J, Wang T, Wang S, Liu J, *et al*. GPX4 Alleviates Diabetes Mellitus-Induced Erectile Dysfunction by Inhibiting Ferroptosis. Antioxidants (Basel, Switzerland). 2022; 11: 1896. https://doi.org/10.3390/antiox11101896.

[46] Nakamura T, Ogawa M, Kojima K, Takayanagi S, Ishihara S, Hattori K, *et al*. The mitochondrial Ca^{2+} uptake regulator, MICU1, is involved in cold stress-induced ferroptosis. EMBO Reports. 2021; 22: e51532. https://doi.org/10.15252/embr.202051532.

[47] Liu F, Cao L, Hu S, Ye H, Wu Q, Wu L. Muscone promotes functional recovery by facilitating microglia polarization into M2 phenotype through PPAR-γ pathway after ischemic stroke. Cellular Immunology. 2023; 386: 104704. https://doi.org/10.1016/j.cellimm.2023.104704.

[48] Zhang P, You S, Ding X, Luan P, Xu J, Cui Q, *et al*. Protective effect and underlying mechanism of muscone on acute cerebral ischemia-reperfusion injury in rats. Journal of Ethnopharmacology. 2023; 308: 116287. https://doi.org/10.1016/j.jep.2023.116287.

[49] Gui Y, Kim Y, Brenna S, Wilmes M, Zaghen G, Goulbourne CN, *et al*. Cystatin C loaded in brain-derived extracellular vesicles rescues synapses after ischemic insult in vitro and in vivo. Cellular and Molecular Life Sciences: CMLS. 2024; 81: 224. https://doi.org/10.1007/s00018-024-05266-4.

[50] Rehman SU, Shah SA, Ali T, Chung JI, Kim MO. Anthocyanins Reversed D-Galactose-Induced Oxidative Stress and Neuroinflammation Mediated Cognitive Impairment in Adult Rats. Molecular Neurobiology. 2017; 54: 255–271. https://doi.org/10.1007/s12035-015-9604-5.

[51] Arboix A, Massons J, García-Eroles L, Targa C, Comes E, Parra O. Clinical predictors of lacunar syndrome not due to lacunar infarction. BMC Neurology. 2010; 10: 31. https://doi.org/10.1186/1471-2377-10-31.